Nonlinear Aeroelastic Analysis of the X-56A Multi-Utility Aeroelastic Demonstrator

Jessica R. Jones[1] and Carlos E.S. Cesnik[2]
University of Michigan, Ann Arbor, MI, 48109, USA

This paper describes the development of a simplified nonlinear aeroelastic model for the Lockheed Martin X-56A Multi-Utility Demonstrator. Equivalent beam stiffnesses and inertias are calculated from a NASTRAN FEM model. Sectional aerodynamic coefficients are also calculated from wind-tunnel verified CFD data and additional X-FOIL results. The information is used within the University of Michigan Nonlinear Aeroelastic Simulation Toolbox (UM/NAST) to create a simplified coupled nonlinear aeroelastic/flight dynamics representation of the X-56A. With this model, various aeroelastic phenomena can be studied including trim, flutter onset, and elastic-rigid body coupling.

Nomenclature

C_D	=	aircraft drag coefficient
c_d	=	airfoil drag coefficient
C_L	=	aircraft lift coefficient
c_l	=	airfoil lift coefficient
C_M	=	aircraft moment coeffient
c_m	=	airfoil moment coeffient
c_n	=	chord of element n
d_i	=	drag in aircraft region i
D	=	aircraft drag
F_i	=	applied force in global frame ($i = X, Y,$ or Z)
f_B	=	first bending frequency
g_n	=	ratio of n-th element chord to the chord of the first element in the region
I_{ij}	=	cross-sectional inertia in local beam coordinate frame
κ_i	=	curvature in the local beam coordinate frame
l_n	=	length of element n
M_i	=	beam internal bending moment in global frame ($i = X, Y,$ or Z)
m_i	=	beam internal bending moment in local frame ($i = 1, 2,$ or 3)
q_{ref}	=	dynamic pressure at reference velocity
R_n	=	reference node at spanwise station n
$R_{\hat{n}}(\varphi)$	=	rotation matrix of angle φ about axis $\hat{n}$
S_{ij}	=	cross-sectional stiffness constant in local beam coordinate frame
T	=	applied torsion moment in global frame
θ	=	rotation in local beam coordinate frame
u,v,w	=	displacement in local beam coordinate frame
V_{ref}	=	reference velocity

---

[1] Graduate Research Assistant, Dept. of Aerospace Engineering, 1052 FXB, 1320 Beal Ave, AIAA Member.
[2] Professor, Dept. of Aerospace Engineering, 3024 FXB, 1320 Beal Ave., AIAA Fellow.

I. Introduction

T HERE has been a recent trend of growing interest in aircraft known as High Altitude Long Endurance (HALE) aircraft. These aircraft are characterized by their ability to loiter at altitudes far higher than conventional cruise altitudes and flight durations that are measured in days and weeks rather than hours. These capabilities uniquely qualify these aircraft for applications previously reserved for satellites, including atmospheric monitoring, intelligence, surveillance, and reconnaissance (ISR) missions, and communications networking. The performance requirements of HALE flight, when applied to a traditional fixed wing configuration, typically result in designs with high aspect ratio, lightweight wing structures with low natural frequencies and significant deformation under normal loading conditions.

The deformation experienced by HALE-type aircraft during trimmed flight is often large enough to be considered geometrically nonlinear, and the elastic frequencies of these light, flexible structures leads to coupling with the rigid body modes, usually short period, phugoid and/or dutch-roll modes. Thus, traditional methods of analyzing fluid-structure interaction, commonly involving linear finite element models coupled with nonlinear, unsteady CFD,[1] are insufficient for the aeroelastic analysis of these aircraft. Improved analysis methods, typically in time domain, that take into account the nonlinear subsystem interactions present during different phases of the aircraft flight are required for full understanding of the its flight dynamics and stability.[2]

Researchers have taken many different approaches to improving the capability of existing aeroelastic tools for the study of very flexible aircraft. A direct approach is to couple nonlinear structural models with nonlinear CFD to provide a high fidelity aeroelastic analysis environment. Garcia, Seber, and Bendiksen coupled nonlinear FEA beam and plate models to CFD to study high aspect ratio wings in transonic flight regimes.[3,4] Cesnik and co-workers coupled a quasi-3D nonlinear structural model with unstructured, deformable CFD to perfom high fidelity analysis of HALE aircraft in compressible flow.[5,6] These high-fidelity methods are very accurate, but are usually quite computationally expensive. For HALE aircraft in low speed flows, this expense is not always warranted. A simplified elastic aircraft representation with unsteady potential flow equations is sufficient to model the nonlinear aeroelastic effects.

Patil, Hodges, and Cesnik combined a nonlinear, intrinsic beam formulation with unsteady, finite-state aerodynamics that captured the coupling between flight dynamic modes and structural trim of a Daedalus-inspired aircraft.[7,8] Building on this work, Patil and Hodges developed the NATASHA simulation, using composite beam theory and Peters' finite-state inflow theory to perform nonlinear trim and stability analysis on flying wing structures.[9,10] Concurrently, Cesnik and co-workers have developed the University of Michigan Nonlinear Aeroelastic Simulation Toolbox (UM/NAST), a nonlinear strain-based beam formulation coupled with Peter's theory to perform time-domain trim, static, and dynamic analysis of nonlinear aeroelastic behavior of a variety of aircraft configurations.[11–14] A significant advantage of these lower-order codes is their speed and ease of which key aeroelastic parameters can be adjusted, making them ideal to support the development of HALE vehicles from initial design to control simulation. However, while the aircraft models used for these codes are simple in comparison to their higher fidelity counterparts, the creation of an accurate model for use in these codes is not a trivial process.

In the typical aircraft design process, a built-up FEM model is used to analyze the structural behavior and some detailed description of the aircraft aerodynamic properties, derived from CFD or wind tunnel data, is combined with it to generate an aeroelastic model. With the rising prevalence of quick, accurate lower-order nonlinear analysis tools, the desire to convert these built-up models into simplified models for use with these tools has grown as well. Singh and Nicols used a NASTRAN model consisting of quadrilateral shells to calculate equivalent beam stiffnesses and inertias of a horizontal stabilizer for use in wind tunnel and flutter analysis.[15] Malcolm and Laird performed a similar procedure on an ANSYS model of wind turbine blades to calculate cross-sectional beam stiffness matrices for use in ADAMS.[16] Smith used the FEM wingbox model of the NASA Common Research Model to develop a beam model of the wing for use in aeroelastic tailoring.[17] Love and co-workers derived a beam model for body freedom flutter analysis in ASWING from the NASTRAN model of the Lockheed Martin Sensorcraft Swept Flying Wing.[18] This paper will combine and build upon these methods to develop a nonlinear beam model of the Lockheed Martin X-56A Multi-Utility Aeroelastic Demonstrator for UM/NAST for use in flutter analysis.

II. The X-56A Multi-Utility Demonstrator

The X-56A Multi-Utility Aeroelastic Demonstrator, also known as the Multi-Utility Technology Testbed is a joint venture among Lockheed Martin Skunk Works, the Air Force Research Laboratory, and NASA's Armstrong Flight Research Center. The goal of the project is to provide a platform to study active flutter suppression

American Institute of Aeronautics and Astronautics

technologies and provide data to advance the state of the art of "performance aggressive" aircraft. The subscale aircraft has an aspect ratio of 14 with a wingspan of 27.8 feet. Its modular wing design allows for flight tests at various payload and wing stiffness configurations, as well as allowing the aircraft to be modified to a joined wing design.[19]

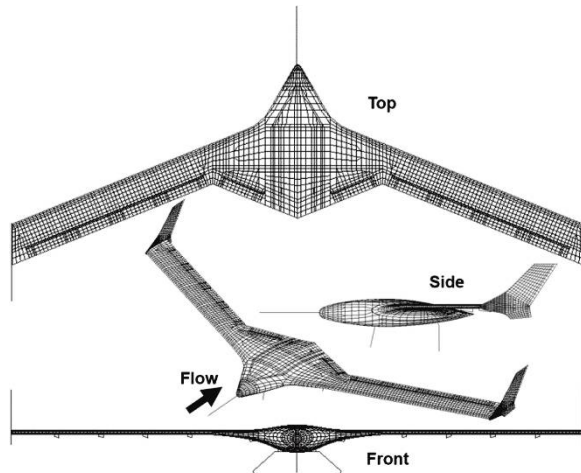**Figure 1. X-56A Multi-Utility Technology Testbed, courtesy of Lockheed Martin**

Figure 2. X-56A baseline FEM model[20]

The initial elastic and inertial properties of the X-56A were provided through a detailed finite element model, illustrated in Figure 2. The model was generated and analyzed by Lockheed Martin with MSC NASTRAN and validated with results from ground vibration tests.[20] Aerodynamic force and moment coefficients for the full aircraft were calculated using nonlinear CFD and verified with wind tunnel tests, and the aircraft outer mold line is provided for the calculation of spanwise aerodynamic properties. These constitute the data from which the X-56A beam model for UM/NAST is created.
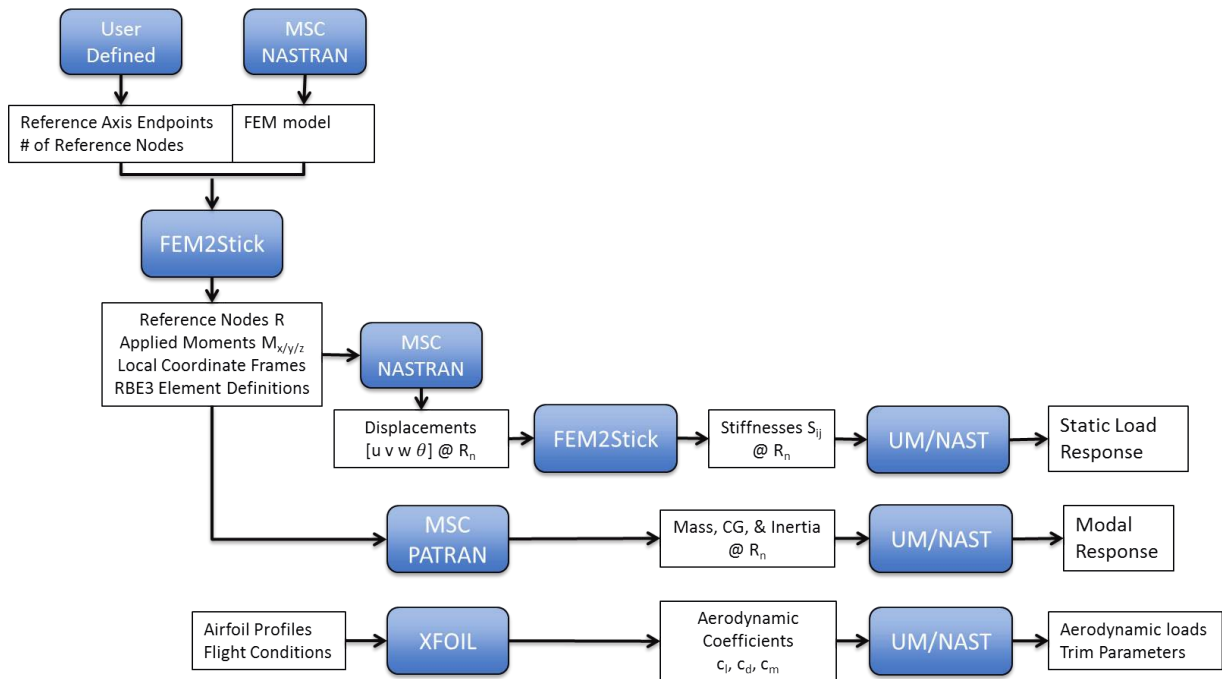

Figure 3. Conversion process from built-up FEM model to UM/NAST beam model

3
American Institute of Aeronautics and Astronautics

III.   Conversion of Built-up Model to Beam Model

In order to convert the detailed aerodynamic and finite element models into a beam-level representation, the cross-sectional elastic, inertial, and aerodynamic properties of the vehicle must be obtained along the span in the regions of interest. Each region of interest is a chordwise strip designated by a reference node. This conversion process distills all of the information of the built-up model into concentrated values relative to the reference node locations. Figure 3 details the information required and the various software tools used in this process.

A built-up FEM model and a CAD model of the X-56A were provided as input data for the conversion process. FEM2STICK, a MATLAB-based software developed by Ben Smith of Aurora Flight Sciences,[17] is used to generate the cross-sectional stiffnesses along a user's selected beam reference line. MSC NASTRAN/PATRAN, a commercial finite element analysis tool, is used to calculate spanwise concentrated inertias from the FEM model, and perform static and modal analyses on the FEM model for conversion and comparison to the UM/NAST beam model. XFOIL is a subsonic airfoil analysis software[20] that is used to calculate the local aerodynamic coefficients from airfoils derived from the wing cross-section. UM/NAST is used to create the beam model from the reference axis, cross-sectional stiffnesses and inertias, and airfoil aerodynamic coefficients. UM/NAST's static analysis feature is used to verify the stiffnesses by calculating the static load response of the beam model to compare against the FEM model. The aero coefficients are verified similarly by comparing the steady-state aerodynamic loads generated by UM/NAST against aircraft aerodynamic loads provided by NASA. UM/NAST's modal analysis feature is used to validate the inertias by comparing the mode shapes and frequencies of the beam model against the FEM model.
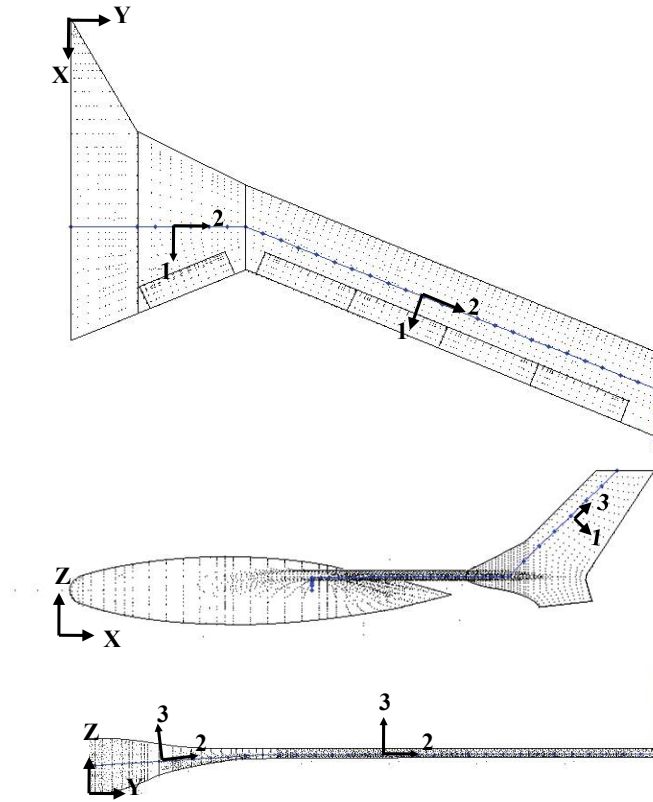

Figure 4. X-56A reference frames

A. Definition of the Reference Axis

To begin the conversion from the built-up model to beam model, a set of 10, 20, 30, and 40 reference nodes are defined along the X-56A wingspan. These reference nodes are evenly distributed along the span at the midchord, and the locus of these points form the beam reference axis. The reference axis, which is not necessarily the elastic axis, is shown in Figure 5. All lengths are normalized by the aircraft's mean aerodynamic chord unless otherwise specified. For each set of reference nodes, the cross-sectional stiffnesses along the span of the wing are generated

American Institute of Aeronautics and Astronautics

and used to determine the response of the wing to a static load in UM/NAST. The reference node set that yields the best static performance will be used to generate the spanwise inertial properties.
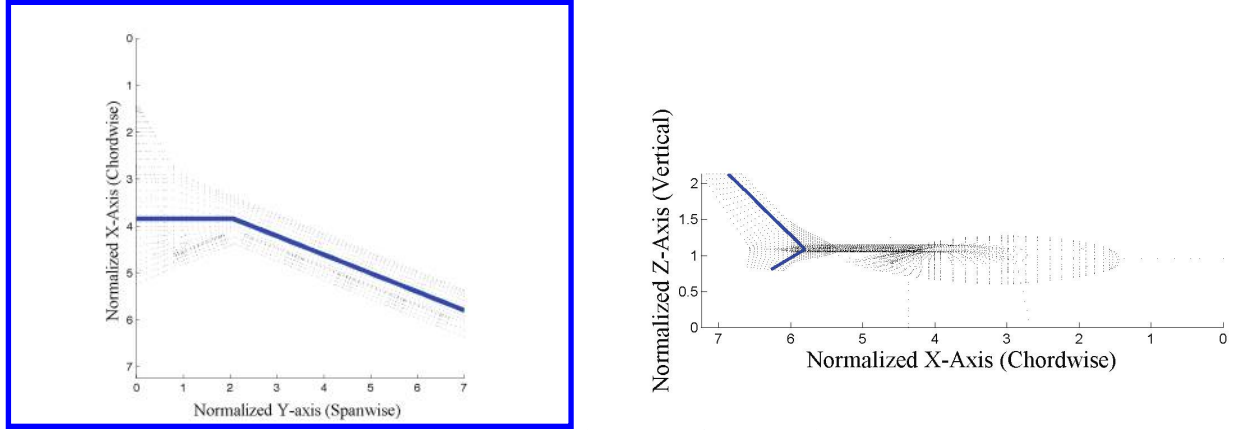

Figure 5. X-56A beam reference axis

B. Creation of Cross-sectional Stiffnesses

The beam moment-curvature relationship is used to calculate the cross-sectional stiffnesses along the wingspan. A moment applied to the wingtip produces curvatures in three perpendicular directions, corresponding to torsion, vertical bending, and inplane bending. The internal, local moments are a coordinate transformation of the applied moments, defined as:

$$\begin{Bmatrix} m_1 \\ m_2 \\ m_3 \end{Bmatrix}_{3x1} = \left[R_{\hat{n}}(\varphi) \right]_{3x3} \begin{Bmatrix} M_X \\ M_Y \\ M_Z \end{Bmatrix}_{3x1} \tag{1}$$

where $R_{\hat{n}}(\varphi)$ represents the rotation matrix from the global reference frame to the local beam reference frame, with a rotation of angle φ about the direction $\hat{n}$.

The relationship between the internal moments and the resulting beam curvatures at a given cross section within the wing can be expressed using a symmetric 3x3 matrix of stiffness constants:

$$\begin{Bmatrix} m_1 \\ m_2 \\ m_3 \end{Bmatrix}_{3x1} = \begin{bmatrix} S_{vertical} & S_{vert/tors} & S_{vert/inpl} \\ S_{vert/tors} & S_{torsion} & S_{tors/inpl} \\ S_{vert/inpl} & S_{tors/inpl} & S_{inplane} \end{bmatrix}_{3x3} \begin{Bmatrix} \kappa_1 \\ \kappa_2 \\ \kappa_3 \end{Bmatrix}_{3x1} \tag{2}$$

The beam curvatures are the spanwise derivatives of the beam twist and bending rates. For geometrically linear, straight beams:

$$\begin{Bmatrix} \kappa_1 \\ \kappa_2 \\ \kappa_3 \end{Bmatrix} = \begin{Bmatrix} w'' \\ \theta' \\ -v'' \end{Bmatrix}, \quad \text{with } (\cdot)' = \frac{\partial}{\partial Y} \tag{3}$$

This equation must be solved at each reference node in order to calculate the representative stiffness of each cross-sectional slice of the built-up model. Since this beam constitutive relationship is linear with respect to the curvatures, it only needs be evaluated once. To automate the stiffness calculation process detailed by Singh and Nicols,[15] FEM2Stick uses a set of user-defined start and end points and chordwise location to define a reference line composed of a desired number of reference nodes. These reference nodes are defined as RBE3 interpolation elements in NASTRAN, thus the displacements and rotations at the reference nodes are not independent, but are

5

American Institute of Aeronautics and Astronautics

representative of the motion of all of the neighboring elements in their region and are given in the local beam coordinate frame.

Three perpendicular moments are defined in the global XYZ frame and applied to the wingtip of the FEM wing model in NASTRAN. These moments and their deformation response are small enough that the linear curvature definition described above is valid. The deformation of the wing is interpolated by the RBE3 elements into local displacements and rotations at each reference node location from which FEM2Stick calculates twist rate and in-plane and vertical bending curvatures using a central finite-difference method. The moment-curvature equation is employed as the next step to generate the cross-sectional torsion and bending stiffnesses and coupling terms at each reference node. As mentioned earlier, four reference node sets—10, 20, 30, and 40 nodes—are considered for the generation of stiffnesses. The spanwise distribution of cross-sectional stiffness constants and coupling terms for each reference node set is shown in Figure 6.

C. Tuning the Stiffnesses

For all four reference node sets, the procedure outlined above is able to capture the overall stiffness distribution of the wing, and the stiffness values all fall within the same order of magnitude. If the structure being analyzed were straight and composed of a homogenous material, all four reference node sets would yield virtually identical stiffness results. However, in addition to the tapered wing-body region and swept main wing, the X-56A wing FEM model contains a variety of internal structures whose effect can be seen as local stiffness spikes in the 20, 30, and 40 node sets, but are absent in the 10-node set. Furthermore, the discretization of the FEM model yields elements with an average width that is 3% of the semispan, which is too coarse for the 40-node discretization. This crowding forces the reference nodes to interpolate information from elements that do not belong to their respective regions, overlapping with neighboring regions and yielding spurious stiffness values as a result. The 30-node discretization is the maximum number of evenly-spaced reference nodes that this FEM model can accommodate, where each reference node region in the wing-body contains a single chordwise column of elements.

The FEM model also includes five control surfaces that compose over 90% of the wing's trailing edge. Each control surface is composed of flexible shell elements and hinges allow them to move independently of the main wing when actuated. During loading, these control surfaces deflect relative to the bending and rotation of the wing reference axis. Although these deflections are extremely small relative to the wing's overall motion, Figure 7 shows that they are major contributors to many of the local stiffness spikes in the inplane and vertical bending stiffnesses. The torsional stiffness is not as strongly affected as the bending stiffness terms.

In order to verify that the static behavior of the FEM model is adequately described by the beam model, the calculated stiffnesses are used to create a massless wing in UM/NAST. Three perpendicular tip loads acting in the X, Y, and Z directions are applied to the both the FEM and UM/NAST wing models, and their responses are compared. The error in wingtip displacement of the UM/NAST model compared to the FEM model is shown in Table 1. Both the 20-node and 30-node versions of the UM/NAST model show good agreement with the FEM model with errors in the tip deflection of less than 1%, so either of these reference node configurations are sufficient to capture the static structural behavior of the wing. The 30-reference node configuration will be used moving forward since its greater node density will be beneficial for deriving the inertias in the next step. A comparison of the UM/NAST 30-node beam and FEM response to static loads is shown in Figure 8.

Table 1. Wingtip displacement error for UM/NAST compared to FEM

Load Applied	Displacement Component	20 nodes	30 nodes
Torsion T	θ	0.9%	0.67%
Inplane Force F_X	v	0.54%	0.66%
Vertical Force F_Z	w	0.4%	0.33%

American Institute of Aeronautics and Astronautics
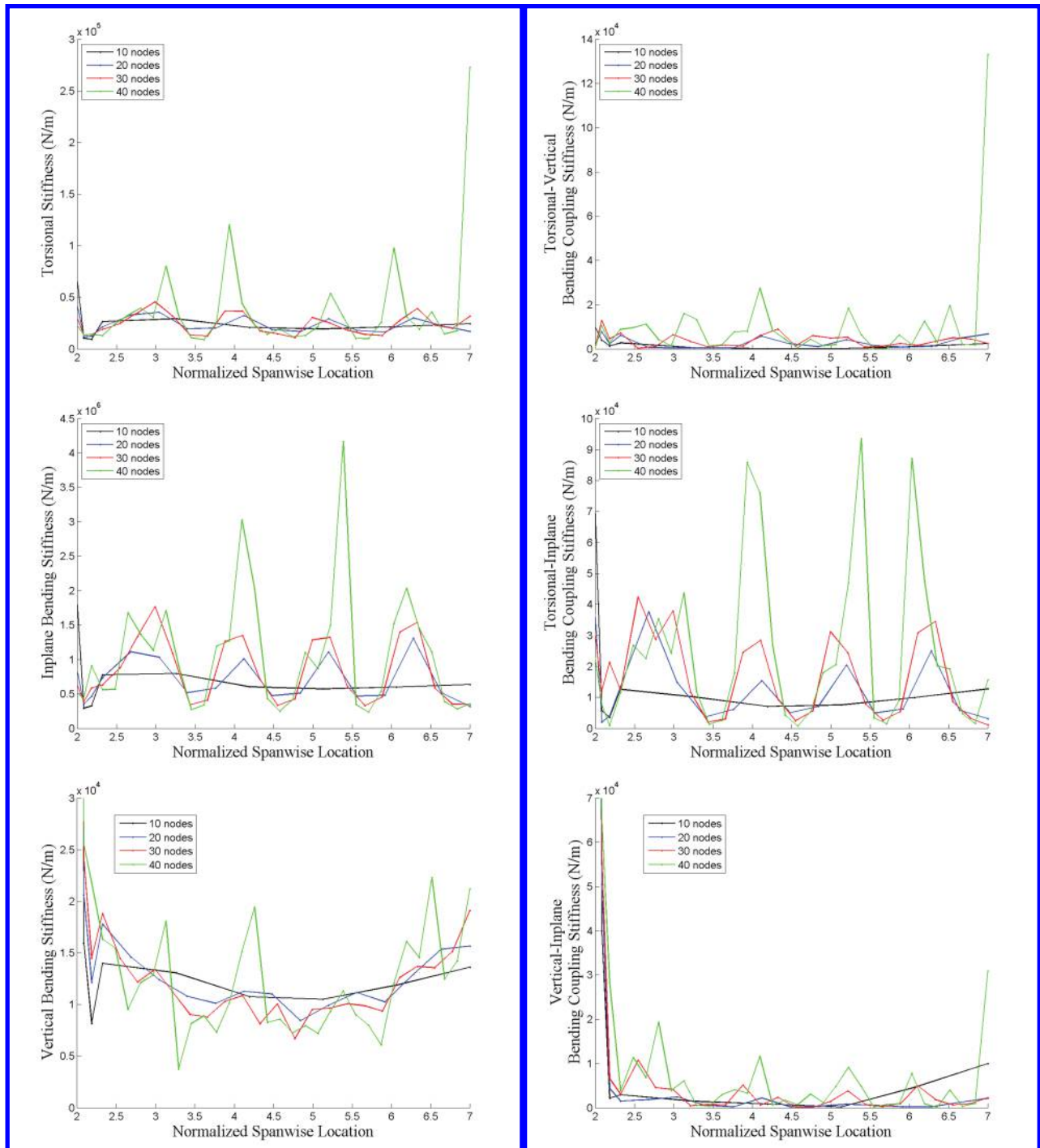
Figure 6. X-56A cross-sectional stiffness constants about the mid-chord reference axis

American Institute of Aeronautics and Astronautics
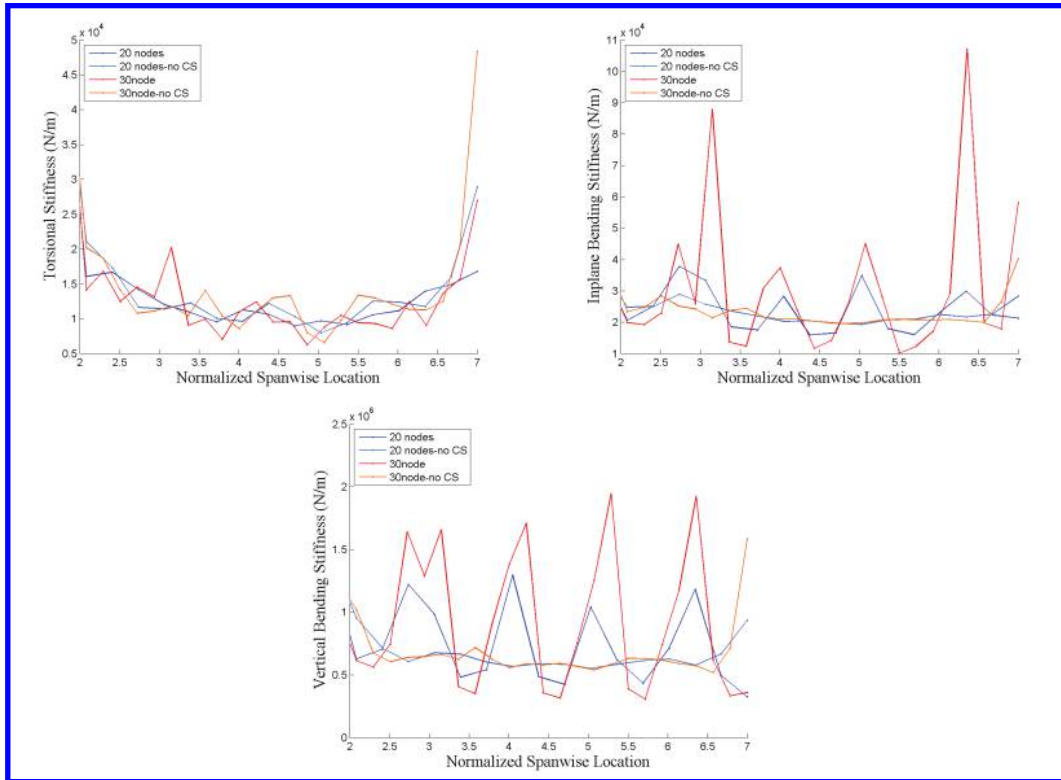
Figure 7. Comparison of stiffnesses with and without control surfaces in the interpolation elements.
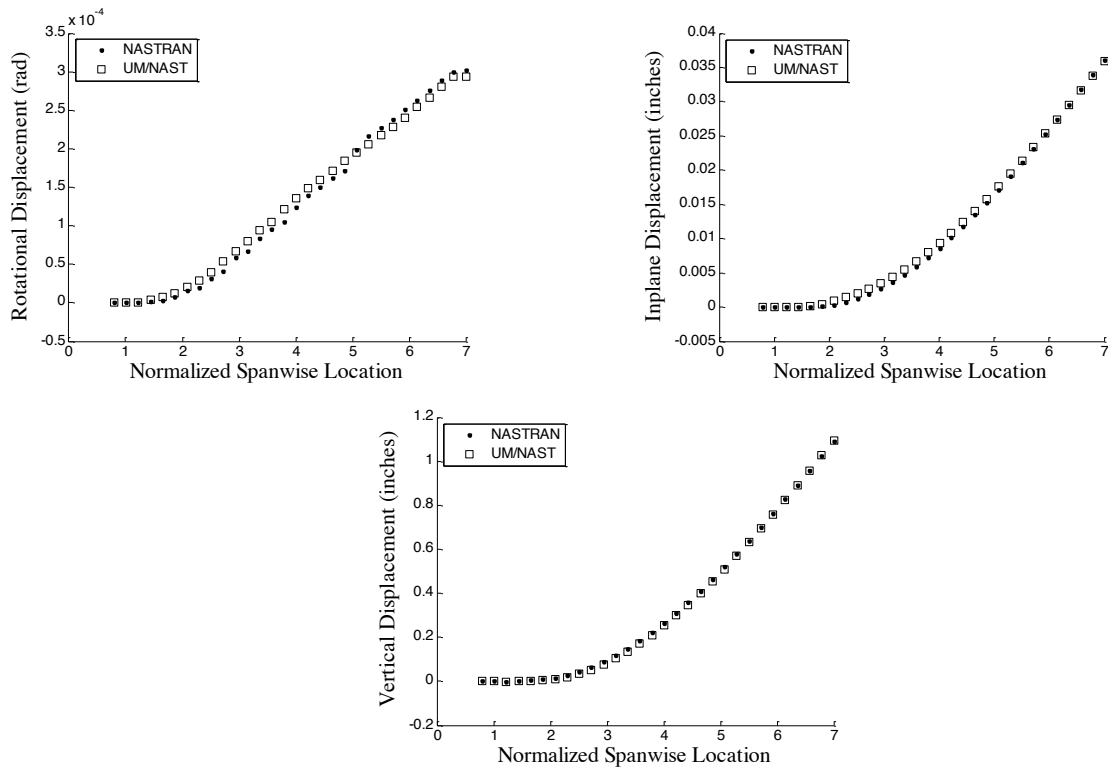
Figure 8. Static analysis results for NASTRAN FEM and UM/NAST beam model; forces applied are (clockwise l-r): tip moment, tip inplane force, and tip vertical force

8

American Institute of Aeronautics and Astronautics

D. Calculation of Cross-sectional Inertias

In order to model inertial properties in UM/NAST, the structural and nonstructural masses and inertias of the FEM model are lumped into concentrated inertias for the beam model. In order to calculate the lumped properties for the reference beam, the Mass Properties tool of MSC Patran is used. Mass regions corresponding to the stations of the 20 and 30 reference node sets are defined, and the mass, center of gravity, and concentrated inertias are calculated for each region. Four additional regions are used to define the inertia of the winglet. The center of gravity of each region becomes the location of a point mass in the UM/NAST model. Figure 9 shows the location of these point masses, which represent the mass of each wing region, relative to the wing reference node positions. Figure 10 and Figure 11 show the spanwise distribution of mass and cross-sectional inertias, respectively. The mass values are normalized by the total mass of the wing. Inertia is measured about the center of gravity in the local 1, 2, and 3 axes, and normalized by the mass-weighted wing reference area. The center of gravity positions are normalized by the aircraft mean aerodynamic chord. A comparison between the wing's total mass and center of gravity is given in Table 2**.**
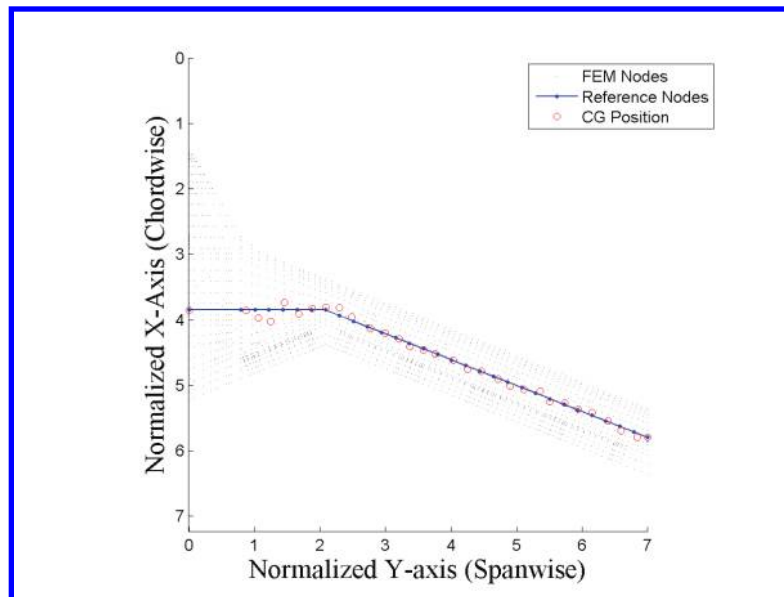

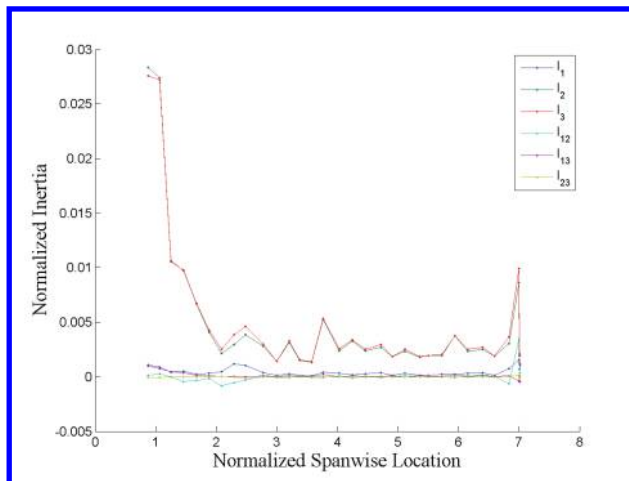**Figure 9. Each reference node has an associated lumped mass and center of gravity**
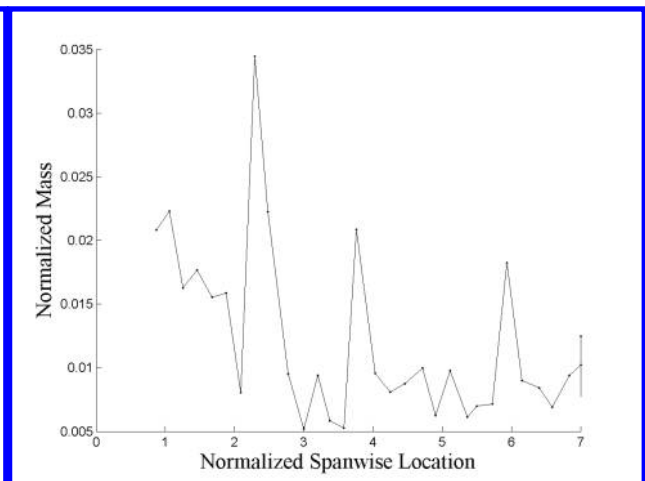

Figure 10. Spanwise inertia distribution

Figure 11. Spanwise mass distribution

9
American Institute of Aeronautics and Astronautics

Table 2. Total mass and center of gravity of the wing

Property	NASTRAN	UM/NAST	%Error
Normalized Mass	100	99.97	0.03%
Normalized CG_X	7.41	7.40	0.11%
Normalized CG_Y	3.69	3.66	0.94%
Normalized CG_Z	4.33	4.44	-2.55%

E. Modal Analysis

Similarly to what was described above regarding the stiffness constants verification against static deflections, the inertia values extracted from the 3D FEM also need to be verified. The inertial properties presented in the previous section were used to generate the initial modal frequencies in UM/NAST, then the frequencies were adjusted by tuning the inertias to match the NASTRAN model, which has been validated with ground vibration tests. Two X-56A models are developed here: Model A incorporates control surface motion in the stiffnesses and models them as rigid beams, while Model B neglects control surface motion altogether. The inertias of Model A are split between the main reference beam and control surface beams. The frequency correlation of the first four modes from NASTRAN and the UM/NAST models are presented in Table 3. The frequencies are normalized against the first vertical bending frequency from the NASTRAN model. The mode shapes are shown in Figure 12.

The control surfaces and winglet participate significantly in many of the lower frequency modes, and the UM/NAST beam models are still able to capture the mode coupling that occurs, even without a detailed model of the dynamics of the control surfaces. The simpler Model B performs better in capturing the modal frequencies and mode coupling, while Model A replicates the shape of the entire mode more closely. For the purposes of this study, the frequencies and mode coupling are more important than the mode shapes themselves, so Model B will be used for the creation of the aerodynamic loads and flutter analaysis.

Table 3. Normalized natural frequencies of NASTRAN and UM/NAST models

Mode Shape	Normalized Frequency			% Error	
	NASTRAN Model	UM/NAST Model A	UM/NAST Model B	UM/NAST Model A	UM/NAST Model B
1st vertical bending	1.00	0.97	0.99	2.89%	0.74%
1st torsion, coupled with vertical bending	4.87	4.63	4.91	4.97%	-0.67%
1st inplane, coupled with vertical bending & torsion	5.28	5.02	5.29	4.87%	-0.20%
2nd torsion, coupled with vertical bending	6.61	6.16	6.51	6.87%	1.52%

IV. Creation of the Aerodynamic Model

Wind-tunnel validated lift, drag, and moment coefficients for the X-56A full aircraft were provided for various angles of attack, sideslip angles, and control surface deflections. Figure 13 shows the aerodynamic coefficients provided for the full aircraft at zero angle of attack and zero sideslip angle, with no control surface deflection, at the reference airspeed V_{ref}.

The local airfoil profile, chord, and incidence angle of the blended-wing-body vary significantly, but linearly, in the first 30% of the span, while the main wing maintains a constant airfoil profile and chord. Seven slices are taken along the span, six in the wing-body region, and one in the main wing, shown in Figure 14. The lift, drag, and moment coefficients versus the stall-normalized local angle of attack for each profile were generated using XFOIL and shown in Figure 15.
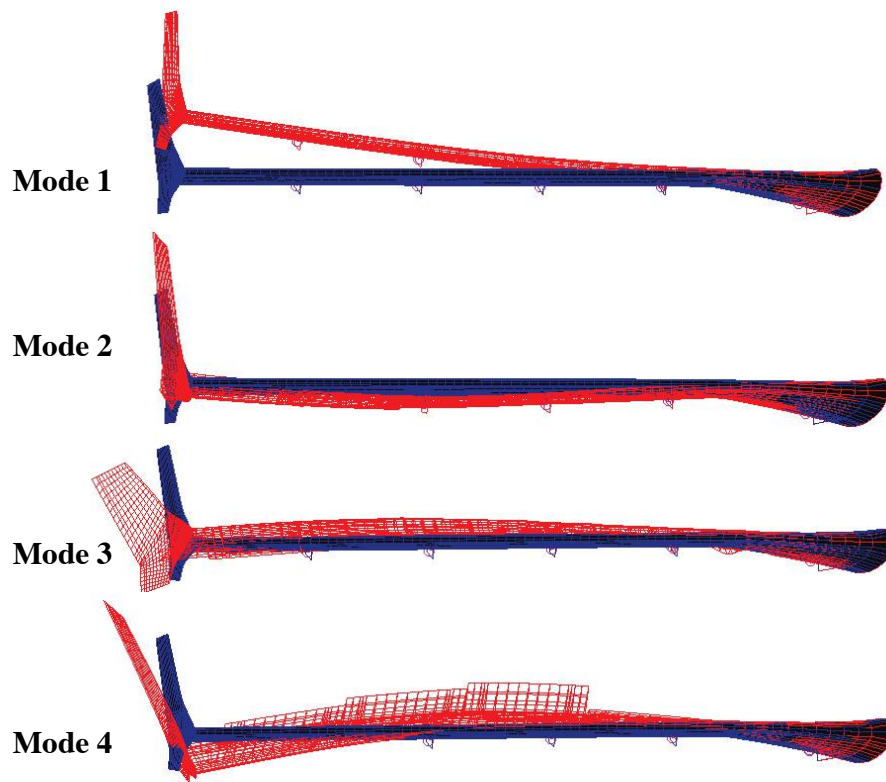
American Institute of Aeronautics and Astronautics

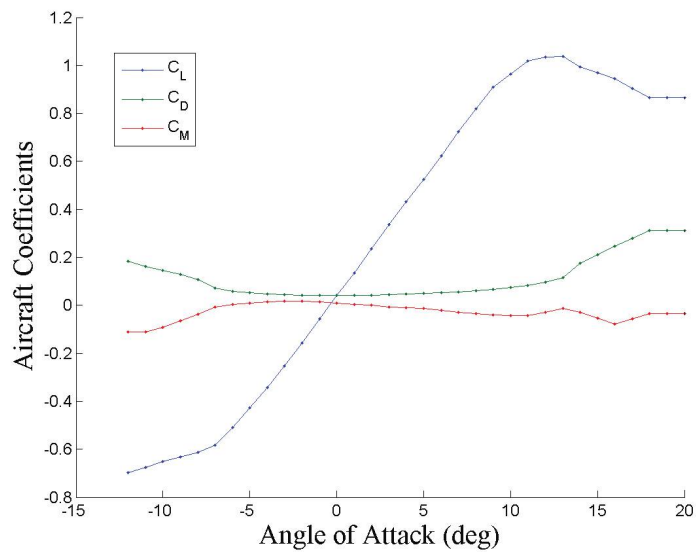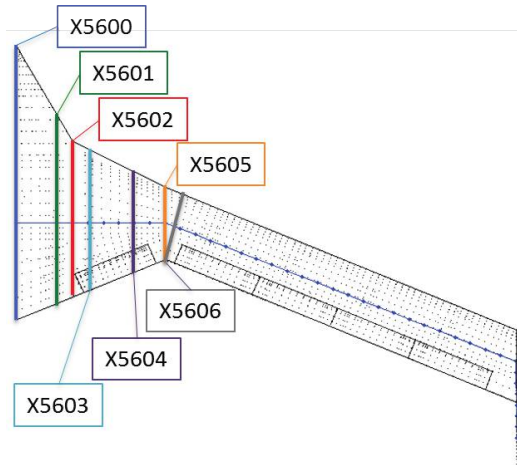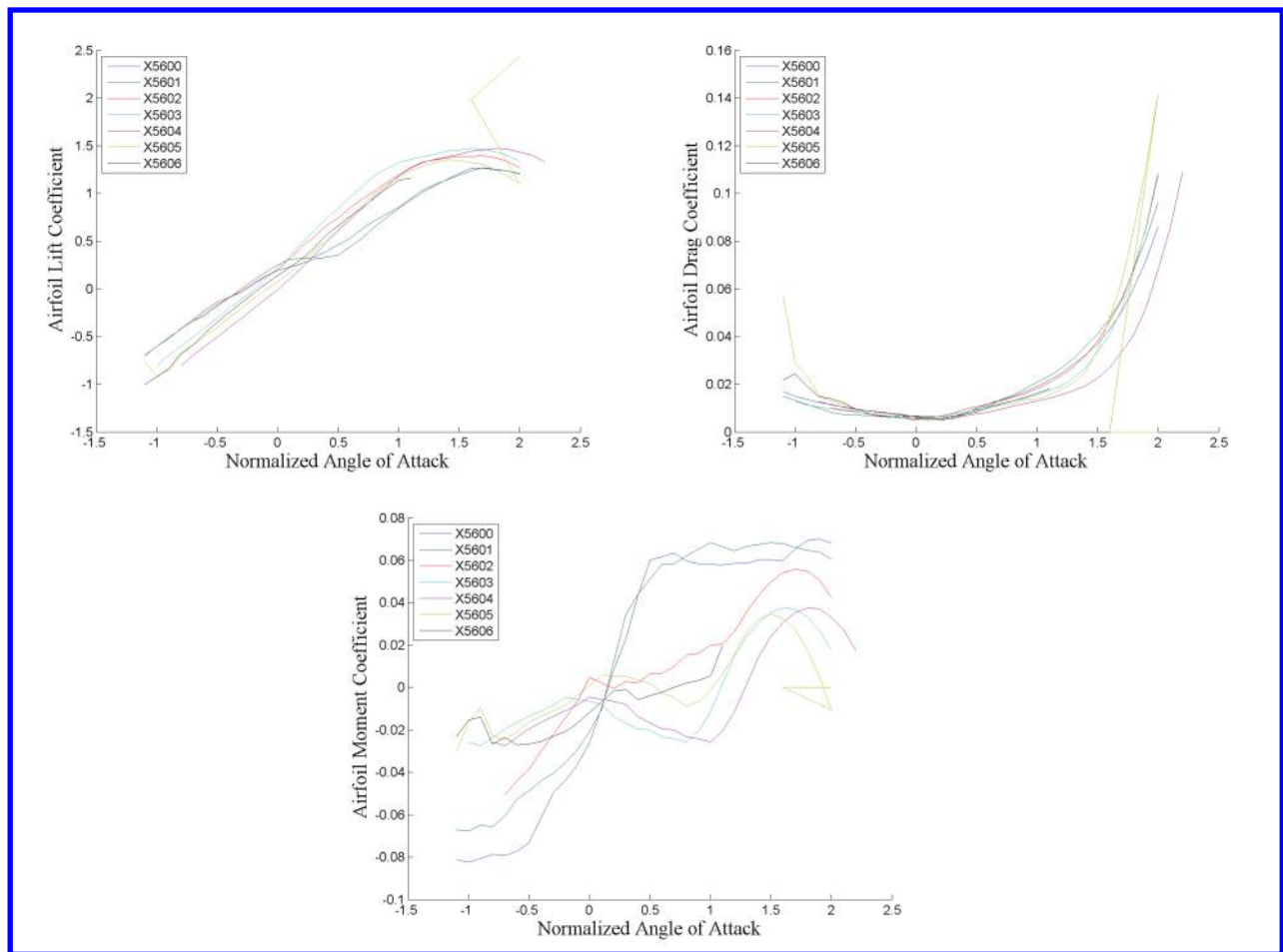**Figure 12. X-56A natural mode shapes**

Figure 13. X-56A aircraft aerodynamic coefficients

Figure 14. Spanwise airfoil stations

Figure 15. Cross-sectional lift, drag, and moment coefficients at different spanwise stations

The UM/NAST aerodynamic solver interpolates these coefficients at every point in the structural beam reference axis and generates the local aerodynamic loads using Peters' finite-state inflow theory. These local loads are then integrated across the span, including the winglet, to generate the full lift, drag, and pitching moment of the aircraft. The lift, drag, and moment distribution is shown in Figure 16, and the aerodynamic loads are assumed to be symmetric about the center of the aircraft. The model used corresponds to Model B from the previous sections.
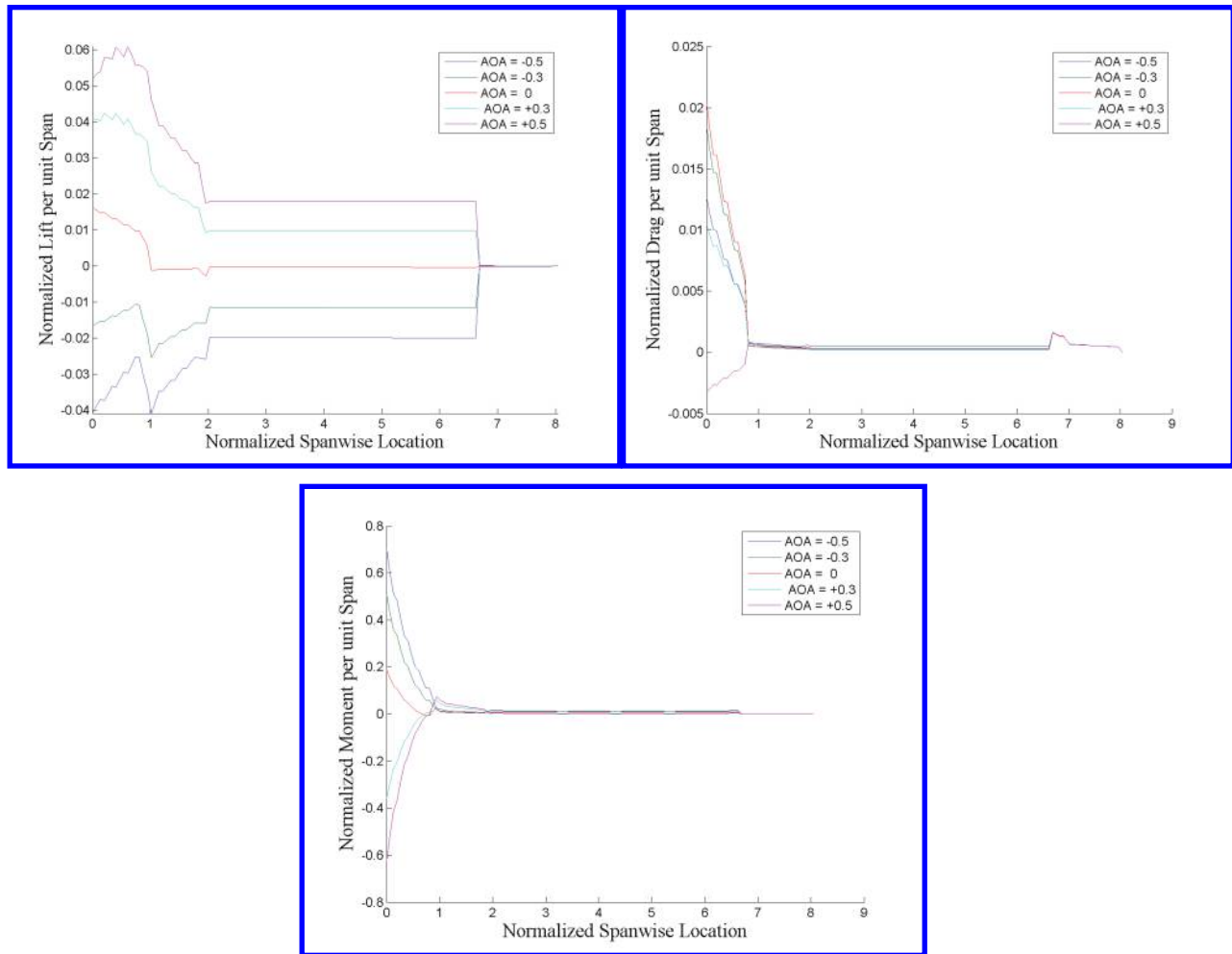
12

American Institute of Aeronautics and Astronautics

Figure 16. Lift, drag, and moment distributions over the semispan of the X-56A UM/NAST (Model B)

A comparison between the lift, drag, and moment of the full aircraft for the wind tunnel test-corrected data and the UM/NAST simulation is shown in

Figure **17**. The total lift of the aircraft matches well between ±5 degrees, while stall begins to set in outside of that range. The aircraft drag from XFOIL viscous drag coefficient underpredicted the total drag on the aircraft, and failed to capture the stall behavior. This is likely due to the drag contributions of the landing gear, engines, and other body-mounted equipment that is not modeled in UM/NAST. The aircraft moment was similarly underpredicted, although the trend matched well due to its close dependence on the lift coefficient. To account for the low aerodynamic loads, a correction was applied to both the moment and drag coefficients to match the aircraft load, and these corrected values are shown in the figure.

The drag correction Δd_i for each region i of the aircraft is expressed with respect to the total aircraft drag delta:

$$\Delta D = D_{test} - D_{NAST} \tag{4}$$

$$\Delta d_i = \Delta D(\frac{d_i}{D_{NAST}}) \tag{5}$$

Each region is composed of n elements, with the chord allowed to vary from element to element to account for the tapering of the wing. The drag coefficient $c_{d,n}$ of each element is weighted by element chord c_n and given as a ratio relative to the drag coefficient of the first element in the region:

$$g_n = c_n \cdot c_{d,n} / c_1 \cdot c_{d,1} \tag{6}$$

13
American Institute of Aeronautics and Astronautics

The element drag coefficients are integrated along the span to yield the region drag coefficient, and rearranging the integral equation yields an expression for the first element drag coefficient, from which all others can be derived, i.e.,

$$\Delta D = \int (\Delta d_i)ds = 0.5 q_{ref} \sum_{n=1}^{N} (l_{n+1} - l_n)(d_n + d_{n+1}) \Rightarrow \quad c_{d,1} = \frac{\Delta d_i}{0.5 q_{ref}(l_2 - l_1)(g_n + g_{n+1})} c_1 \tag{7}$$

Replacing the drag and drag coefficients in Eqs. (4-6) with the moment and moment coefficient yields the correction equations for the aircraft moment. Even without additional information about the spanwise coefficients, these corrections are able to approximate the spanwise loads.

V. Dynamic Aeroelastic Analysis

The UM/NAST model created in Sections II through IV is a simplified representation of the X-56A aircraft, and it is able to replicate the elastic, modal, and aerodynamic behavior of the fully built-up model. A trim configuration was generated using as parameters the body angle of attack, control surface deflection, and point forces that simulated the thrust of the engines. The wing deformation and aerodynamic load distribution of the aircraft for several trimmed configurations are shown in Figure 18.
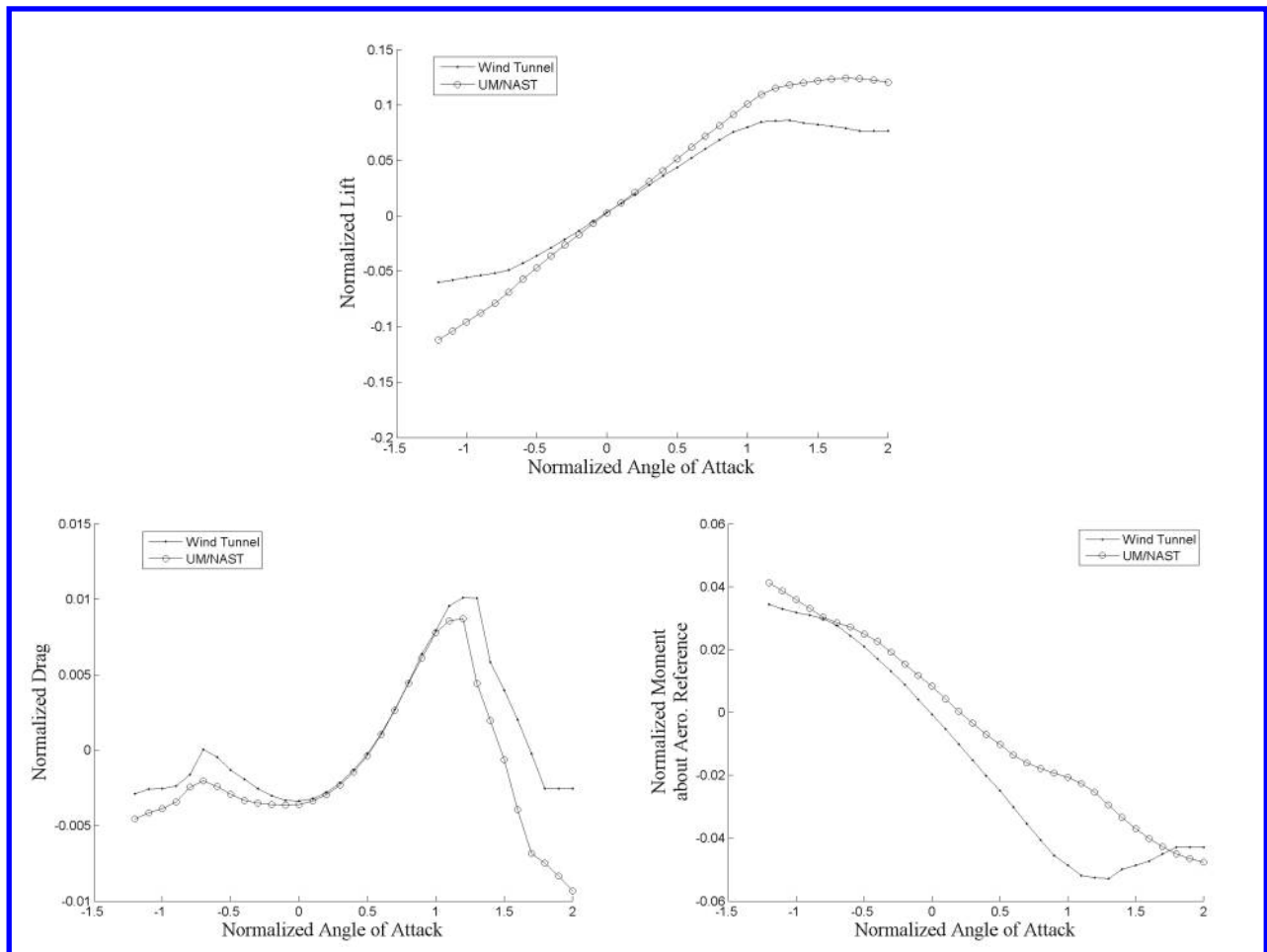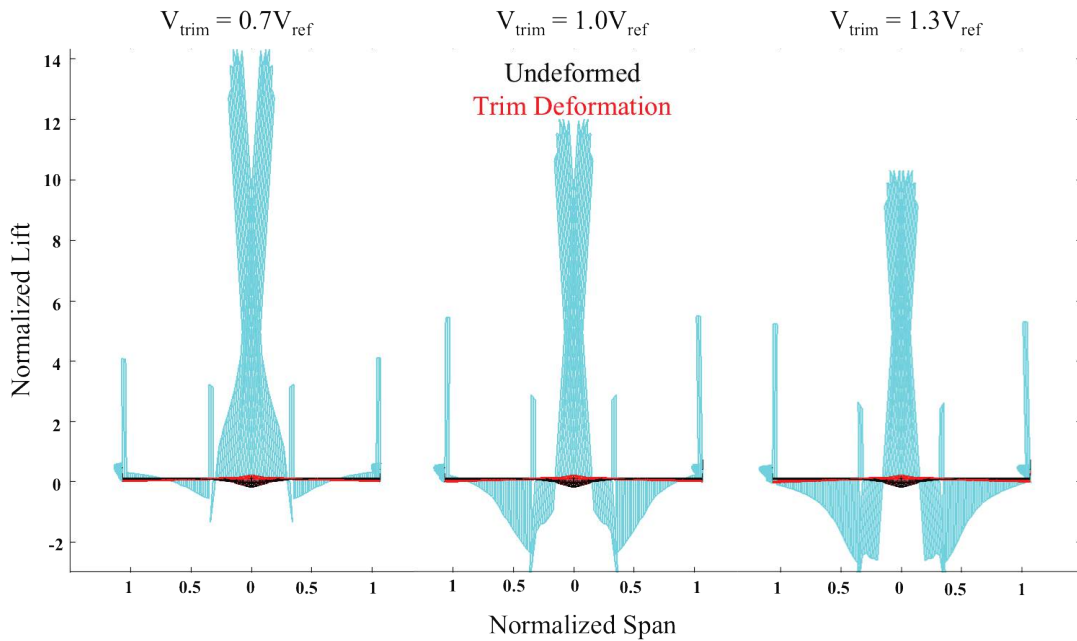

Figure 17. Comparison of wind tunnel aerodynamic loads with the X-56A UM/NAST model

V_trim = 0.7V_ref   V_trim = 1.0V_ref   V_trim = 1.3V_ref

**Figure 18. Lift distribution under trimmed deflected shape**

A root locus plot showcasing the approach to the flutter boundary is shown in Figure 19. The damping and frequency as a function of speed for the flight regimes around the flutter point are shown in Figure 20. The frequencies are normalized by the frequency of the first bending mode f_B, damping is normalized by the damping at V_{ref}, and velocity is normalized by V_{ref}. The flutter boundary is $1.47V_{ref}$. The flutter mode is a body freedom flutter composed of the first torsion mode, first inplane, and first vertical bending elastic modes coupled with the rigid-body pitch degree of freedom. The initial normalized frequency of this mode is $5.32f_B$, which rises to $5.5f_B$ at the flutter boundary.
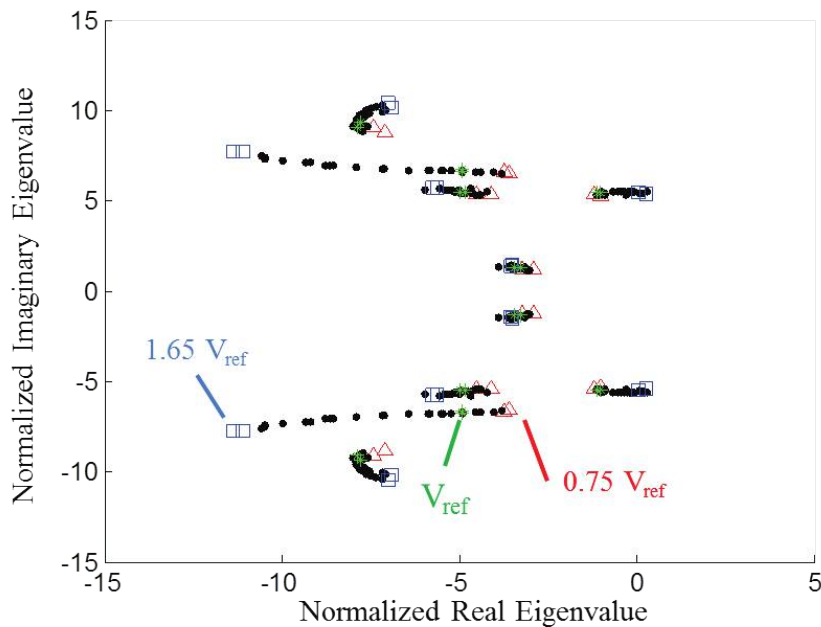
Figure 19. Root Locus of the X-56A rigid body and elastic modes

15

American Institute of Aeronautics and Astronautics
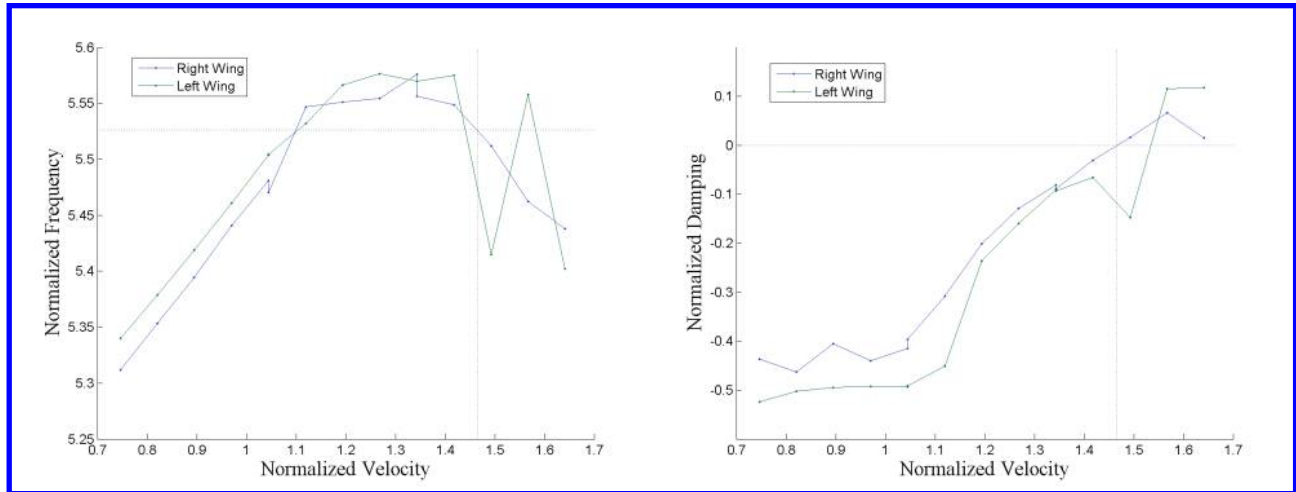
Figure 20. X-56A flutter response
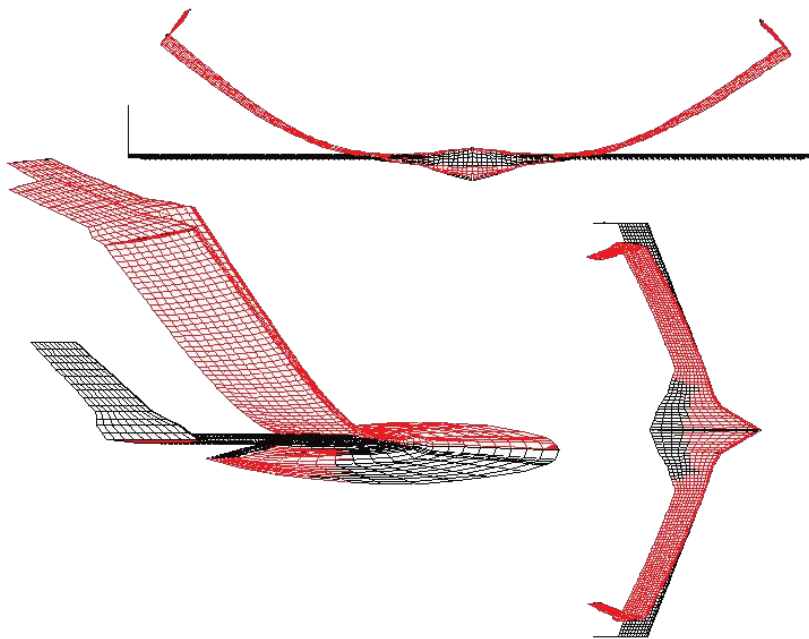
Figure 21. Flutter mode is body pitch coupled with symmetric wing bending and torsion elastic modes

VI. Concluding Remarks

This paper presented the results of a detailed procedure for converting a built-up aircraft model into a simplified aeroelastic model suitable for input into a reduced-order nonlinear aeroelastic solver. The X-56A Multi-Utility Aerolastic Demonstrator served as the test model for the procedure, while UM/NAST performed the nonlinear simulations. Structural and inertial data for the X-56A was obtained through a GVT-validated FEM model. Aerodynamic data was provided in the form of CAD models of the aircraft's outer mold line and lift, drag, and moment coefficients from CFD that were validated by wind tunnel tests. The resulting beam model consisted of 30 reference nodes distributed evenly along the span. The cross-sectional stiffnesses and inertias calculated about each reference node were verified using the UM/NAST static and modal solvers, respectively. The simplified model was able to replicate the deformations resulting from static loads, and the modal frequencies were also within 2% for the first four modes. The aerodynamic loads were subject to more error due to the lack of information about the

16

American Institute of Aeronautics and Astronautics

spanwise distribution, so approximations were made to match the aerodynamic loads generated in UM/NAST to the loads measured in the wind tunnel tests. This nonlinear aeroelastic model was used to conduct a trim and flutter analysis of the X-56A. Future work will investigate the effects of multiple stiffness and payload configurations on the X-56A trim state and flutter response.

Acknowledgments

References

1 Gupta, K., "Development of a finite element aeroelastic analysis capability," *Journal of Aircraft*, vol. 33, 1996, pp. 995–1002.

2 Noll, T. E., Brown, J. M., Perez-davis, M. E., Ishmael, S. D., Tiffany, G. C., and Gaier, M., *Investigation of the Helios Prototype Aircraft Mishap- Volume I Mishap Report*, 2004.

3 Garcia, J. a., "Numerical Investigation of Nonlinear Aeroelastic Effects on Flexible High-Aspect-Ratio Wings," *Journal of Aircraft*, vol. 42, 2005, pp. 1025–1036.

4 Seber, G., and Bendiksen, O. O., "Nonlinear Flutter Calculations Using Finite Elements in a Direct Eulerian-Lagrangian Formulation," *AIAA Journal*, vol. 46, 2008, pp. 1331–1341.

5 Palacios, R., Cesnik, C. E. S., and Fellow, A., "Static Nonlinear Aeroelasticity of Flexible Slender Wings in Compressible Flow," *46th AIAA/ASME/ASCE/AHS Structures, Structural Dynamics and Materials Conference*, 2005, pp. 1–10.

6 Hallissy, B. P., and Cesnik, C. E. S., "High-fidelity Aeroelastic Analysis of Very Flexible Aircraft," *Proceedings of 52rd AIAA/ASME/ASCE/AHS/ASC Structures,Structural Dynamics and Materials Conference*, Denver, CO: American Institute of Aeronautics and Astronautics, 2011, pp. 1–22.

7 Patil, M. J., Hodges, D. H., and Cesnik, C. E. S., "Nonlinear Aeroelastic Analysis of Aircraft with High-Aspect-Ratio Wings," *Journal of Aircraft*, 1998, pp. 1–13.

8 Patil, M. J., Hodges, D. H., and S. Cesnik, C. E., "Nonlinear Aeroelasticity and Flight Dynamics of High-Altitude Long-Endurance Aircraft," *Journal of Aircraft*, vol. 38, Jan. 2001, pp. 88–94.

9 Patil, M. J., and Hodges, D. H., "Nonlinear Aeroelastic Analysis of Complete," *Journal of Aircraft*, vol. 37, 2000, pp. 753–760.

10 Chang, C. S., Hodges, D. H., and Patil, M. J., "Flight Dynamics of Highly Flexible Aircraft," *Journal of Aircraft*, vol. 45, May 2008, pp. 538–545.

11 Cesnik, C. E. S., and Su, W., "Nonlinear Aeroelastic Modeling and Analysis of Fully Flexible Aircraft," *Proceedings of 46th AIAA/ASME/ASCE/AHS/ASC Structures,Structural Dynamics and Materials Conference*, Austin, TX: American Institute of Aeronautics and Astronautics, 2005, pp. 1–27.

12 Shearer, C. M., and Cesnik, C. E. S., "Nonlinear Flight Dynamics of Very Flexible Aircraft," *Journal of Aircraft*, vol. 44, Sep. 2007, pp. 1528–1545.

13   Su, W., and S. Cesnik, C. E., "Nonlinear Aeroelasticity of a Very Flexible Blended-Wing-Body Aircraft," *Journal of Aircraft*, vol. 47, 2010, pp. 1539–1553.

14   Cesnik, C. E. S., Senatore, P. J., Su, W., Atkins, E. M., and Shearer, C. M., "X-HALE: A Very Flexible Unmanned Aerial Vehicle for Nonlinear Aeroelastic Tests," *AIAA Journal*, vol. 50, Dec. 2012, pp. 2820–2833.

15   Singh, Ashok K., Nichols, C. W., "Derivation of an Equivalent Beam Model from a Structural Finite Element Model," *The MSC 1988 World Users Conference Proceedings, Vol.1*, 1988, p. Paper No. 14.

16   Malcolm, D. J., and Laird, D. L., "Extraction of equivalent beam properties from blade models," *Wind Energy*, vol. 10, 2007, pp. 135–157.

17   Smith, B., *Aeroelastically Tailored Wing Structures (ATWIST)*, Manassas, VA: 2013.

18   Love, M. H., Zink, P. S., Wieselmann, P. a., and Youngren, H., "Body Freedom Flutter of High Aspect Ratio Flying Wings," *46th AIAA/ASME/ASCE/AHS/ASC Structures, Structural Dynamics, and Materials Conference*, 2005, pp. 1–23.

19   Beranek, J., Nicolai, L., Buonanno, M., Burnett, E., Atkinson, C., Holm-hansen, B., and Flick, P., "Conceptual Design of a Multi-utility Aeroelastic Demonstrator," *10th AIAA Aviation Technology, Integration, and Operations (ATIO) Conference*, Fort Worth, Texas: American Institute of Aeronautics and Astronautics, 2010, pp. 1–15.

20   Li, W. W., and Pak, C., "Mass Balancing Optimization Study to Reduce Flutter Speeds of the X-56A Aircraft," *Journal of Aircraft*, vol. 3, 2015, pp. 1–7.

This article has been cited by:

1. Vishvas S. Suryakumar, Arun S. Mangalam, Yogesh Babbar, Thomas W. Strganac. A Load-Based Feedback Approach for Distributed Aeroservoelastic Control . [Citation] [PDF] [PDF Plus]